Vol. 14, pp. 161–171 (2017)
doi: 10.2142/biophysico.14.0_161

Biophysics and Physicobiology

https://www.jstage.jst.go.jp/browse/biophysico/

Regular Article

Analysis of an ATP-induced conformational transition of ABC transporter MsbA using a coarse-grained model

Naoki Arai[1], Tadaomi Furuta[1] and Minoru Sakurai[1]

[1]*Center for Biological Resources and Informatics, Tokyo Institute of Technology, Yokohama, Kanagawa 226-8501, Japan*

Recieved October 19, 2017; accepted November 2, 2017

Upon the binding of ATP molecules to nucleotide binding domains (NBDs), ATP-binding cassette (ABC) exporters undergo a conformational transition from an inward-facing (IF) to an outward-facing (OF) state. This molecular event is a typical example of chemo-mechanical coupling. However, the underlying mechanism remains unclear. In this study, we analyzed the IF→OF transition of a representative ABC exporter, MsbA, by solving the equation of motion under an elastic network model (ENM). ATP was represented as a single node in ENM or replaced by external forces. When two ATP nodes were added to the ENM of the IF state protein, the two NBDs dimerized; subsequently, the two transmembrane domains opened toward the extracellular side, resulting in the formation of the OF structure. Such a conformational transition was also reproduced by applying external forces, which caused the rotational motion of the NBDs instead of the addition of ATP nodes. The process of the conformational transition was analyzed in detail using cross-correlation maps for node-node interactions. More importantly, it was revealed that the ATP binding energy is converted into distortion energy of several transmembrane helices. These results are useful for understanding the chemo-mechanical coupling in ABC transporters.

Corresponding author: Minoru Sakurai, Center for Biological Resources and Informatics, Tokyo Institute of Technology, B-62 4259 Nagatsuta-cho, Midori-ku, Yokohama, Kanagawa 226-8501, Japan.
e-mail: msakurai@bio.titech.ac.jp

Key words: ABC exporter, elastic network model, protein conformational transition, nucleotide binding domain, transmembrane domain

ABC transporters constitute one of the largest superfamilies of integral membrane proteins that are found in all three domains of life (bacteria, archaea, and eukarya) [1–3]. These ABC transporters are divided into importers and exporters, which allow substrates to be imported into or exported out of the cytoplasm, respectively. Diverse substrates are transported by ABC transporters, e.g., lipids, peptides, ions, and drugs [2,4]. Thus, they are responsible for multidrug resistance (MDR), which has recently become one of the most important problems in medicine [5,6].

Hereafter, we focus on ABC exporters unless otherwise noted. Canonical ABC transporters share a common structural organization, comprising two nucleotide-binding domains (NBDs) that bind and hydrolyze ATP in the cytoplasm and two transmembrane domains (TMDs) that form the translocation pathway for substrates [7,8] (Fig. 1). The TMDs consist of 12 transmembrane (TM) helices, and each TMD has six TM helices. The TMDs make contact with the NBDs through coupling helices (CHs) that are located in two intracellular loops (ICL1 and ICL2) [8] (Fig. 1 and Supplementary Fig. S1). These CHs are embedded in grooves on the surface of the NBD.

◀ ***Significance*** ▶

Upon the binding of ATP to nucleotide binding domains (NBDs), ATP-binding cassette (ABC) exporters undergo a conformational transition from an inward-facing (IF) to an outward-facing (OF) state. This is a typical example of chemo-mechanical coupling. Here, the IF→OF transition of an ABC exporter, MsbA, was studied by solving the equation of motion under an elastic network model, where ATP was represented as a single node. It was found that 1) the twisting motion of the NBDs is indispensable for causing the opening of transmembrane domains, 2) ATP binding energy is converted into distortion energy of several transmembrane helices.

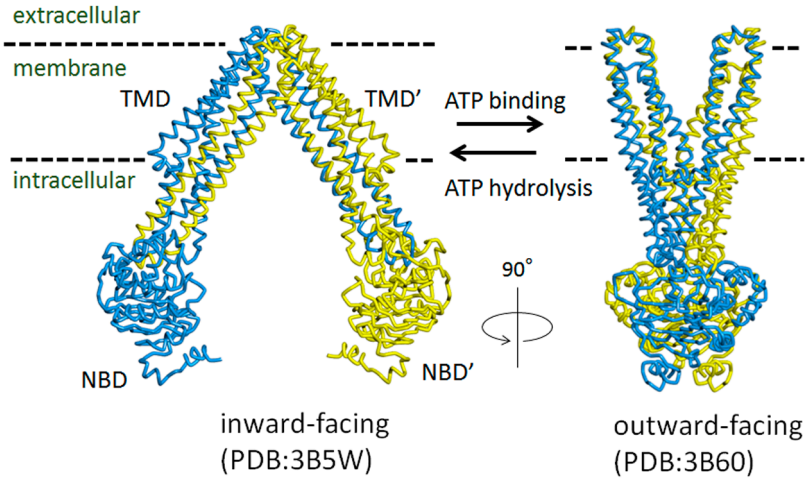

Figure 1 Inward-facing (IF) and outward-facing (OF) structures of MsbA as a typical example of ABC exporters. Blue and yellow chains correspond to chain A and chain B, respectively.

The basic reaction cycle of ABC exporters is thought to consist of a series of several steps [8–12]. In an ATP-free (open apo) state, the protein adopts an inward facing (IF) conformation, where the two NBDs are separated and, consequently, the TMDs are open to the cytoplasmic side (Fig. 1). Upon the binding of two ATP molecules, the NBDs dimerize, which may push the coupling helices toward each other; consequently, the TMDs convert into an outward-facing (OF) conformation (Fig. 1). Upon the hydrolysis of ATP, the reverse transition occurs to reset the transporter to the ground state for the next step: the NBD dimer opens, consequently pulling the CHs outward and causing the conversion to an inward-facing conformation (Fig. 1). The first half process is thought to be driven by the free energy of ATP binding to the NBDs and the second half by the energy of ATP hydrolysis. However, there is much less understanding of the mechanism by which the energy of ATP is converted into the mechanical motions of the protein or, in other words, the mechanism of the chemo-mechanical coupling.

Molecular dynamics (MD) simulations and free energy calculations are powerful tools with which to investigate the structure and mechanism of ABC transporters [13,14]. However, the IF↔OF conformational transition is beyond the timescales allowed by conventional all-atom MD. Instead, enhanced sampling MD methods with bias potentials such as targeted MD (tMD) [15] and umbrella sampling [16] are useful for exploring the atomic details of a large-scale conformational transition if the structures of the initial and final states are both known. An early X-ray study determined the structures of a bacterial ABC lipid flippase, MsbA, in different states, including IF and OF conformations [17]. Weng *et al.* applied tMD to elucidate the OF→IF transition pathway of MsbA [18]. The resultant MD trajectory revealed a clear spatiotemporal order of the conformational movements. Moradi and Tajkhorshid developed a novel approach based on designing an extensive initial search for system-specific reaction coordinates and using non-equilibrium simulations [19] and found that the twisting motions of the NBDs are coupled to the open-close motions of the TMDs, which suggested a novel hypothesis for the conformational dynamics of ABC exporters termed the ‘doorknob’ mechanism [20]. Another strategy to overcome the sampling problem and describe the large-scale conformational changes of proteins is to employ coarse-grained representations of the protein and/or environment models such as elastic network models (ENMs) [21,22], where the elastic forces, acting on the particles, obey Hooke’s law. Recently, Xie *et al.* applied an adaptive anisotropic network model to the problem of the allosteric transition of MsbA and obtained results consistent with the above doorknob mechanism [23].

The above studies based on several enhanced conformational sampling methods have provided invaluable information on the pathway of the IF↔OF transition of MsbA as an example of an exporter. However, these studies provide no direct answer to the first question about the mechanism of the chemo-mechanical coupling in ABC transporters, in short, the role of ATP. To answer this question, one must elucidate how the protein responds to an external perturbation from ATP. Mikhallov and his coworkers successfully analyzed nonlinear conformational relaxation dynamics of proteins by solving the nonlinear equation of motion under the ENM approximation for the proteins [24–26]. In addition, they successfully analyzed how motor proteins respond to the application of external forces. This coarse-grained method, hereafter called nonlinear ENM, is expected to be applicable to the problem of the large conformational transition of ABC exporters. In our recent study on the dimerization of the NBDs of a maltose transporter, we revealed that a large downhill free energy gradient is generated by the binding of ATP to the NBDs; in other words, a strong attractive

force is generated between the ATP-bound NBDs [27]. In this study, we analyze the IF→OF transition in MsbA using the nonlinear ENM method and reveal how the force generated by ATP binding is converted into the motion of the TMDs, leading to an outward-facing structure.

Materials and Methods

Elastic Network Model (ENM)

Each amino acid residue is represented by a bead (node), the position of which is identical to the position of the Cα atom. A network is specified by indicating the equilibrium positions of all nodes. Two nodes are connected by an elastic spring (link) if the equilibrium distance between them is sufficiently small (<8 Å). The elastic forces, acting on the nodes, obey Hooke's law.

To construct the ENM of MsbA, we first obtained the X-ray structure of the IF state from PDB (3B5W). MsbA is a homodimer that consists of two elongated chains (A and B) that are related by two-fold molecular symmetry. Each chain involves an NBD and a TMD that consists of six helices, TM1-TM6 (Table 1 and Supplementary Fig. S1). Hereafter, the two NBDs are discriminated as NBD and NBD', and similarly, the structural components of chain B are discriminated by adding a prime such as TM1'. According to the X-ray structure, the twelve helices are divided into two bundles, each of which involves six helices (Fig. 1). Hereafter, each bundle is called a "wing". The way of dividing the twelve helices into the two wings is different between the IF and OF states, as shown in Table 2 and Supplementary Figure S1. In the IF state, TM1–TM3 and TM6 from chain A and TM4'–TM5' from chain B pack into one wing, and TM1'–TM3' and TM6' from chain B and TM4–TM5 from chain A form the other wing. Upon going from the IF to OF state, the packing of the TM helices is rearranged as shown in Table 2 and Supplementary Figure S1. Then, a considerable problem is encountered in our ENM. If the six helices in each wing in the IF state are connected by elastic springs according to the above distance criterion, the IF→OF transition (helices rearrangement) could never occur because the springs cannot be cut. To avoid this problem, the inter-helix connections that hinder the OF formation were removed in advance in the IF state.

Table 1 Structural components and their corresponding amino acid residues

	amino acid residues
TM 1 (1')	10–57
TM 2 (2')	58–110
TM 3 (3')	121–166
TM 4 (4')	167–213
TM 5 (5')	223–274
TM 6 (6')	275–324
NBD (NBD')	325–560

Table 2 TM helices constructing each wing in the IF and OF states

		TM helices involved
IF	$wing_1^{IF}$	1, 2, 3, 6, 4', 5'
	$wing_2^{IF}$	1', 2', 3', 6', 4, 5
OF	$wing_1^{OF}$	1, 2, 3', 4', 5', 6'
	$wing_2^{OF}$	1', 2', 3, 4, 5, 6

Equation of motion

In the overdamped limit, the velocity of a node is proportional to the sum of elastic forces applied to it. If $\boldsymbol{R}_i^0$ are the equilibrium positions of the nodes and $\boldsymbol{R}_i(t)$ are their actual coordinates, the dynamics can be described by [24,26]

$$\gamma\dot{\boldsymbol{R}}_i = -\sum_{j=1}^{N} A_{ij} k \frac{\boldsymbol{R}_i - \boldsymbol{R}_j}{|\boldsymbol{R}_i - \boldsymbol{R}_j|}(|\boldsymbol{R}_i - \boldsymbol{R}_j| - |\boldsymbol{R}_i^0 - \boldsymbol{R}_j^0|) + \boldsymbol{F}_i \quad (1)$$

where A is the adjacency matrix, which has the elements $A_{ij}=1$, if $|\boldsymbol{R}_i^0 - \boldsymbol{R}_j^0| < 8$ Å and $A_{ij}=0$ otherwise. This cutoff distance value is different from that (10 Å) used in the original papers. $\boldsymbol{F}_i$ is an external force that is applied to node i. According to the original papers [26], the dependence on the stiffness constant k of the strings and the viscous friction coefficient γ of the nodes can be removed by an appropriate rescaling of the elastic energy and time. After such rescaling the forces become measured in units of length (Å). A force with the strength of 1 Å applied to a single elastic link induces its elongation by 1 Å. Here, the molecular dynamics step size was $\Delta t=0.01$ according to a previous report [25].

One can examine how the protein responds to the application of an external force of arbitrary orientation to each single residue in important functional regions. In the original paper [26], conformational responses of myosin to the application of forces to individual residues in its principal functional regions were systematically investigated. As a result, it was found that static forces applied to the myosin tail induce opening and closing of the front door of the nucleotide binding pocket. In this study, we performed similar simulations by applying the static forces given by eqs. (2)–(6) to the NBDs of MsbA.

Definition of the x-, y- and z-axes

To define the external forces below, we here define the x-, y- and z-axes, as shown in Figure 2. The x-axis is one connecting the center of mass (COM) of NBD and the COM of NBD', and the origin of the coordinate system was placed at the middle point of this axis. The y-axis is taken to be perpendicular to the x-axis through the origin and to be directed to the hinge of the TMDs in the IF state. The z-axis was taken to be perpendicular to the x- and y-axes through the origin.

External forces

In our previous study on the NBDs of maltose transporter [27], an attractive force was observed between the separated

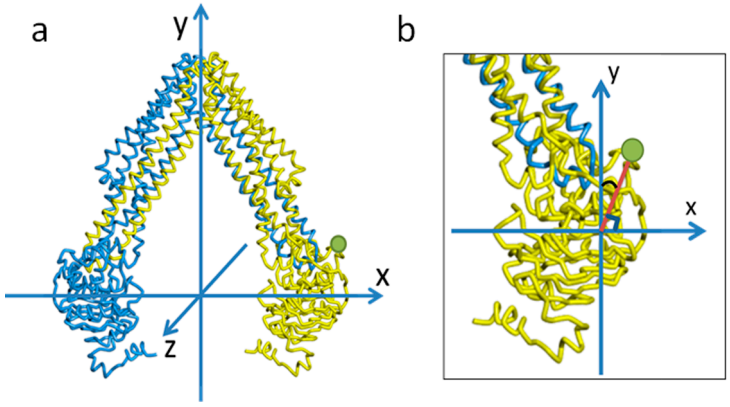

Figure 2 a. Definition of the x-, y- and z-axes. b. Close-up view to explain the rotation about the x-axis. The green circle indicates the COM position of the marker residues (Asn468–Leu480) that were chosen to measure the rotation of the NBDs (see the subsection "Effect of the rotational forces" in Results). The red line indicates the line perpendicular to the x-axis through the green circle. For convenience, the y-axis is shifted to the intersection of this red line and the x-axis. The rotation about the x-axis was measured by the angle made between the y-axis and the red line.

NBDs by the binding of an ATP molecule to each NBD. In this study, we show that such a force can be simulated by sequential application of the following two types of external forces to the NBD parts of the full MsbA.

The first is a force that causes translational motions of NBD and NBD' along the x-axis. Hereafter, this force is denoted the translational force. To node *i* of NBD, the following force was applied:

$$\boldsymbol{F}_i = a\frac{\sum_j^{NBD}\boldsymbol{R}_j - \sum_j^{NBD'}\boldsymbol{R}_j}{\left|\sum_j^{NBD}\boldsymbol{R}_j - \sum_j^{NBD'}\boldsymbol{R}_j\right|} \tag{2}$$

where a is a parameter that determines the magnitude of force $\boldsymbol{F}_i$ and was taken to be 0.002. To node i of NBD', a force with the same magnitude as $\boldsymbol{F}_i$ was applied in the opposite direction, that is, $-\boldsymbol{F}_i$. Thus, these forces are expected to cause the closing of the two separated NBDs in the IF state (Fig. 1).

The second force is one that causes rotation of each NBD about the x-, y- or z-axis. Hereafter this force is denoted as rotational force and is given by

$$\boldsymbol{F}_i = \boldsymbol{S}^{axis}\boldsymbol{X}_i^{axis} \quad (\text{for node } i \text{ in } NBD,\ axis = x \text{ or } y \text{ or } z) \tag{3}$$

where $\boldsymbol{X}_i^{axis}$ is the vector drawn from the COM of each NBD to node i, with components of (R_i^x, R_i^y, R_i^z). The rotational force about the x- or z-axis in NBD' is given by $-\boldsymbol{F}_i$, and that about the y-axis is identical to $\boldsymbol{F}_i$. The x, y and z components of $\boldsymbol{S}^{axis}$ are given as follows:

$$\mathbf{S}^x = \begin{bmatrix} 1 & 0 & 0 \\ 0 & cos\Delta\varphi & -sin\Delta\varphi \\ 0 & sin\Delta\varphi & cos\Delta\varphi \end{bmatrix} \tag{4}$$

$$\mathbf{S}^y = \begin{bmatrix} cos\Delta\varphi & 0 & sin\Delta\varphi \\ 0 & 1 & 0 \\ -sin\Delta\varphi & 0 & cos\Delta\varphi \end{bmatrix} \tag{5}$$

$$\mathbf{S}^z = \begin{bmatrix} cos\Delta\varphi & -sin\Delta\varphi & 0 \\ sin\Delta\varphi & cos\Delta\varphi & 0 \\ 0 & 0 & 1 \end{bmatrix} \tag{6}$$

where $\Delta\varphi$ is the rotation angle (degree) of node i around the x (or y or z) axis and was changed by a step of 3.0×10^{-5} degree during MD simulation.

Addition of the ATP node

In the ATP-bound state of ABC transporters, two ATP molecules are sandwiched between two NBDs. In more detail, each ATP molecule binds to the Walker A motif on one NBD and to the signature motif on the other NBD (NBD') [8]. In the present ENM, such a bound ATP molecule was considered one node. Then, we searched for the amino acid residues that should be linked to the ATP node as follows. In the OF structure of MsbA (PDB ID: 3B60), AMP-PNP instead of ATP binds to the two NBDs. Accordingly, we measured the distance between the C2' atom of the AMP-PNP molecule (Fig. 3a) and the Cα atoms of its surrounding amino acid residues and searched for amino acid residues whose Cα atoms are located within 8 Å from the C2' atom of the AMP-PNP. As a result, we found the nine residues shown in Figure 3b and linked their nodes to the ATP node with elastic strings. Finally, the ATP node was placed at the COM of these nine residues. The equilibrium lengths between the ATP node and these nine nodes were assumed to be identical to those in the X-ray structure (PDB ID: 3B60).

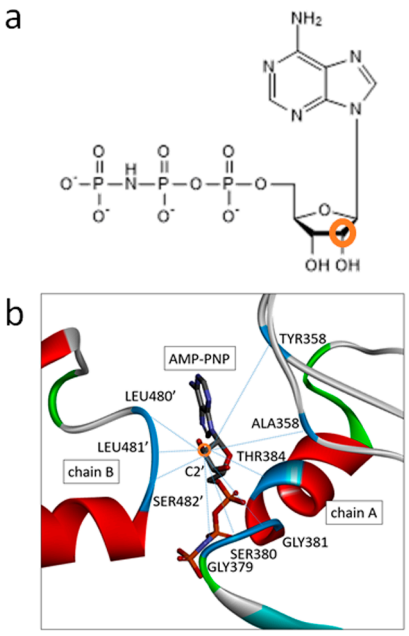

Figure 3 a: The structure of AMP-PNP and the position of the C2' atom (orange circle). b: Nine amino acid residues located within 8 Å from the C2' atom of AMP-PNP in the X-ray structure (PDBID: 3B60). The newly added elastic strings (links) are represented by blue dotted lines.

Correlated motion

To reveal the motional correlation between two nodes i and j, the following cross-correlation was evaluated:

$$C_{ij}^k = \frac{\boldsymbol{v}_i^k \cdot \boldsymbol{v}_j^k}{|\boldsymbol{v}_i^k|\,|\boldsymbol{v}_j^k|} \tag{7}$$

$$\boldsymbol{v}_i^k = \boldsymbol{R}_i(k) - \boldsymbol{R}_i(k-1) \quad (k=0, \ldots, n) \tag{8}$$

where n is the total MD steps and $\boldsymbol{R}_i(k)$ is the position of node i in the kth snapshot structure, and $\boldsymbol{R}_i(0)$ is the initial position at time = 0. The cross-correlation value ranges from –1 to 1. Positive values indicate that the residues move in the same direction, and negative values indicate that they move in the opposite direction.

Internal energy

The internal energy of the system at a given snapshot was defined as distortion energy measured from a given reference structure. The contribution of each node to the distortion energy is given by

$$E_i^k = \sum_{j=1}^N A_{ij} \frac{|R_{ij}^k - R_{ij}^0|^2}{2} \tag{9}$$

where R_{ij}^k and R_{ij}^0 are the distances between nodes i and j in the kth snapshot and the reference structure, respectively.

Root mean square deviation (RMSD)

The RMSD of a protein structure A with respect to a given reference structure B was evaluated by

$$\mathrm{RMSD(A, B)} = \sqrt{\frac{1}{N}\sum_{i=1}^N (A_i - B_i)^2} \tag{10}$$

where A_i and B_i are the coordinates of node i in structures A and B, respectively.

Results

Effect of the translational forces

We first solved the equation of motion (eq. (1)), to which the translational forces (eq. 2) were added. As expected, translational motions were observed for the two NBDs, the inter-COM distance of which was 50 Å in the initial structure (3B5W). Consequently, the distance between the COMs of the two NBDs was down to 30 Å, which is very close to the inter-COM distance (29.4 Å) in the X-ray structure of the OF state (PDB: 3B60). When the inter-COM distance became shorter than 30 Å, the directions of the translational forces were reversed, resulting in an opening motion of the NBDs. After that, when the inter-COM distance was beyond 30 Å, the forces were again reversed. Such direction changes of the forces were repeated until the total number of MD steps was 50×10^5. Consequently, the inter-COM distance of the NBDs converged to almost the same value as that obtained for the experimental OF structure.

We examined what degree of opening of the TMDs is induced solely by the translational motions of the NBDs. For this purpose, we defined the angle (θ) made between axis 1 on $\mathrm{wing}_1^{\mathrm{OF}}$ and axis 2 on $\mathrm{wing}_2^{\mathrm{OF}}$, where axis 1 (2) is the axis connecting the base and top of $\mathrm{wing}_1^{\mathrm{OF}}$ ($\mathrm{wing}_2^{\mathrm{OF}}$), respectively, and the base and top of each wing is the COM of the several amino acid residues listed in Table 3.

In Figure 4, the angle θ is plotted against MD steps, where the blue dotted line corresponds to the angle (29.3°) observed for the X-ray structure of the OF state. A kink appears at step 20×10^5, which corresponds to the first turning point from closing motion to opening motion of the NBDs. At the final step of 50×10^5, θ is 15.4°, which is closer to that of the X-ray IF structure (16.9°) than that of the OF state. Therefore, the opening of the TMDs was not observed by applying only the translational forces (eq. (2)).

Effect of addition of ATP nodes

Next, we added ATP nodes as virtual ATP molecules to the

Table 3 The amino acid residues specifying the bottom and top of axes 1 and 2

	bottom	top
axis 1	110(TM2), 121(TM3'), 213(TM4'), 223(TM5')	57(TM1), 58(TM2), 166(TM3'), 167(TM4'), 274(TM5'), 275(TM6')
axis 2	110(TM2'), 121(TM3), 213(TM4), 223(TM5)	57(TM1'), 58(TM2'), 166(TM3), 167(TM4), 274(TM5), 275(TM6)

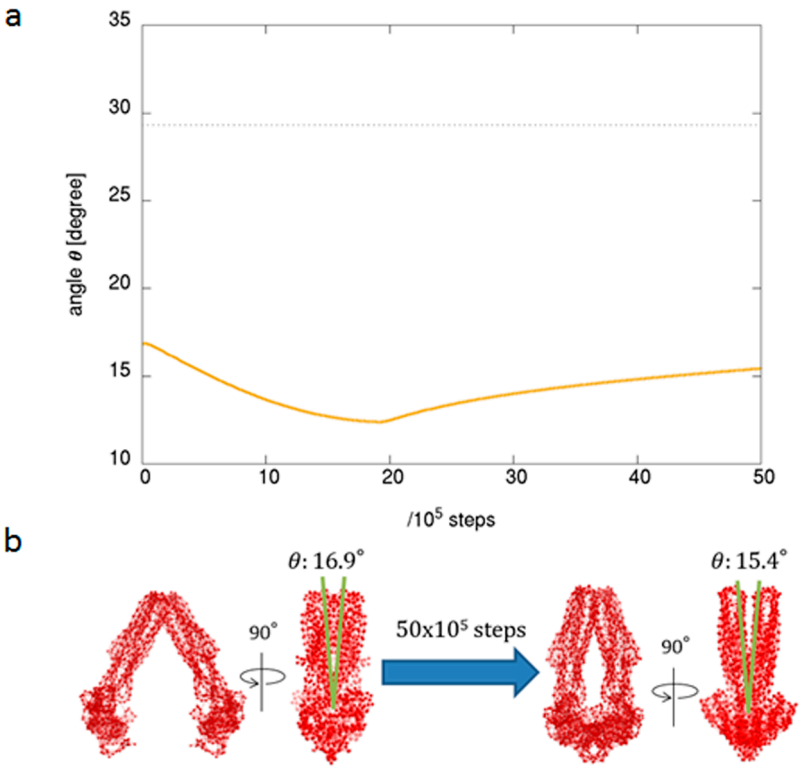

Figure 4 a: Change of the angle θ by applying translational forces (eq. 2) to the NBDs. The abscissa indicates the MD step. b: Illustration of the initial structure (left) and the final structure (right) at step 50×10^5.

elastic network of the above final structure at step 50×10^5, which is hereafter denoted as the NBD-closed structure. The newly added elastic forces drove the system toward another state. After 50×10^5 steps of the simulation, θ increased to 26.0°, which is close to the experimental value of 29.3°. Therefore, by adding the ATP nodes, the IF→OF transition was successfully reproduced.

Effect of the rotational forces

The above observations (Figs. 4 and 5) suggest that ATP binding might generate a type of force that differs from the translational force (eq. (2)) and can ultimately cause the IF→OF transition of the TMDs. What type of NBD motions were caused by ATP binding? Inspection of the final structure in Figure 5 indicated that rotational motions occurred between the NBDs. To examine to what extent each NBD was rotated around the x-, y- or z-axis, we chose a set of amino acid residues (Asn468–Leu480) as a marker: their COM (the green point in Fig. 2b) is fully separated from the center of the NBD. The rotation angle φ_x around the x-axis was measured as the angle between the line perpendicular to the x-axis through this green point and the y-axis. The rotation around the y- or z-axis was also measured in a similar way. The results are summarized in Table 4 and Supplementary Figure S2. In both the simulation and the experimental data, a considerable degree of rotation occurs around each axis, which might be an origin of the opening of the TMDs.

To examine the relationship between the rotation angle φ and the angle θ, we tested the extent to which the angle θ is changed by applying rotational forces (eqs. (3)–(6)). These forces are given as functions of the angle φ. We changed this variable by 3.0×10^{-5} per MD step until its total change reached 5°, 10° or 15°. Then, the angle was fixed to the final value, but the MD simulation was continued until the 50×10^5 th step. The results are summarized in Table 5. For example, when the rotational force was continuously applied until the rotation around the x-axis reached 5°, 10° or 15°, the angle θ increased to reach 26.1°, 35.4° or 43.4°, respectively. The TMDs opened to an angle θ value comparable to the experimental OF structure (θ=29.3°) already in the case of the smallest rotation (5°) of angle φ. In contrast, regardless of the final angle of φ, the force applied about the y- or z-axis exerted no significant influence on angle θ relative to its initial value of 15°.

On the basis of these observations, we can conclude that the elastic forces generated by addition of the ATP nodes mainly causes twisting of the two NBDs around the x-axis, leading to an increase of angle θ (significant opening of the TMDs).

Analysis of the correlated motions

To elucidate the role of ICLs and the detailed process of the rearrangement of the TM helices (Table 2, Supplementary Fig. S1) during the IF→OF transition, we analyzed the

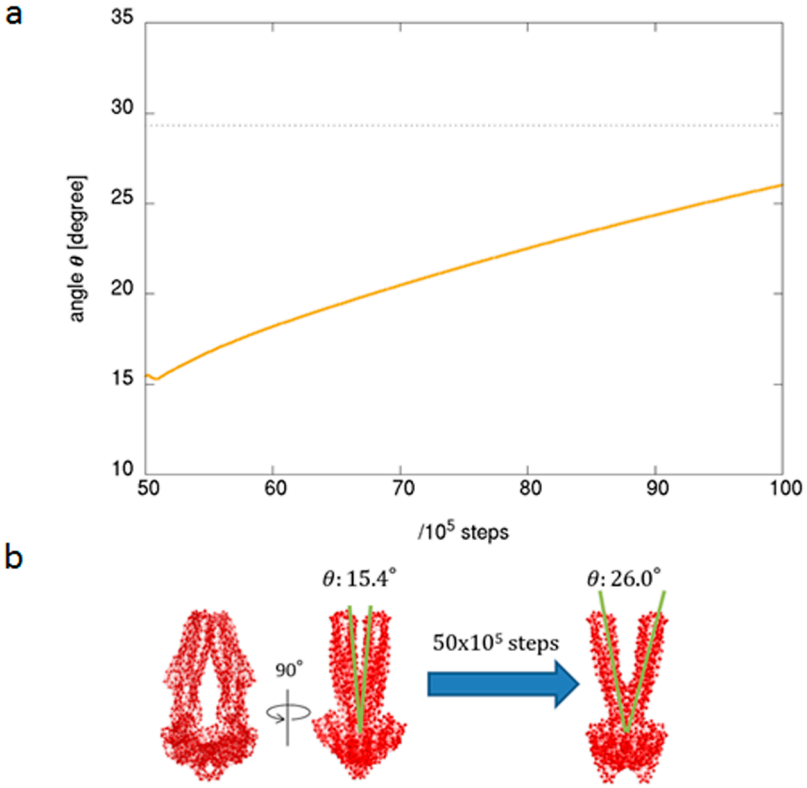

Figure 5 a: Change of the angle θ caused by the addition of ATP nodes. The abscissa indicates the MD step. The MD simulation started from the NBD-closed structure (at step 50×10^5) in Figure 4. b: Illustration of the initial structure (left), identical to the structure in Figure 4b (right), and the final structure at step 100×10^5 (right).

Table 4 Rotation angle of NBD caused by the addition of the ATP node and comparison with the corresponding X-ray data

	Nonlinear ENM MD			X-ray diffraction		
	NBD-closed[1]	Final[2]	increment	IF[3]	OF[4]	increment
φ_x	51.82	59.52	7.70	49.70	60.14	10.44
φ_y	85.97	112.40	26.43	92.65	129.97	37.32
φ_z	4.38	34.50	30.12	2.67	46.92	44.25

[1] Structure at the 50×10^5th step in Figure 4. [2] Structure at the 100×10^5th step in Figure 5. [3] PDB 3B5W structure. [4] PDB 3B60 structure.

Table 5 The final angle θ (degree) reached by applying rotational force $\boldsymbol{F}$ around the x-, y- or z-axis

Direction of the applied force	Total change of angle φ (degree)		
	5	10	15
x	26.1	35.4	43.4
y	15.2	14.0	12.8
z	14.1	12.6	13.6

inter-node correlated motions according to eqs. (7) and (8). Then, we divided the total MD trajectory $0\sim100\times10^5$ steps (the sum of the MD steps shown in Figs. 4 and 5) into 100 intervals, which means that k in eq. (7) was taken to be 0~100. In what follows, we discuss the correlated motions at several representative points.

Figure 6a and 6b show the correlation maps at k=3 and 21, respectively, where the abscissa and ordinate both are partitioned into the structural units involved in both chains A and B instead of the node numbers. At k=3, the protein does not yet undergo significant structural change and the initial experimental IF structure was maintained well. As shown in Table 2, the two wings ($wing_1^{IF}$ and $wing_2^{IF}$) are formed by sets of (TM1, TM2, TM3, TM6, TM4' and TM5') and (TM1', TM2', TM3', TM4', TM5 and TM6), respectively. In accordance with these facts, strong positive correlation (red) is found for the TM helix pair within the same wing, while highly negative correlation (blue) is found for the TM helix pair between the different wings (see the regions surrounded by black squares). ICL1 is the loop connecting TM2 and TM3; thus, its motion has a strong positive correlation with those of these TM helices. Similar correlation is observed between ICL2 and helices TM4 and TM5 linked via ICL2.

At k=21, the two NBDs closely approached each other, whereas the TMDs remained in the IF state (Fig. 4). As a result, the pattern of the correlated motion at this stage was significantly changed from that at k=3 (Fig. 6b). However, the inter-TM helix correlations remained positive within the

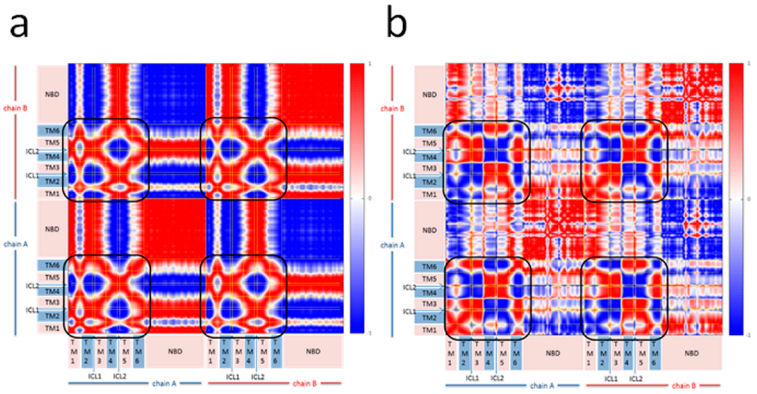

Figure 6 Correlation maps at k=3 (a) and 21 (b).

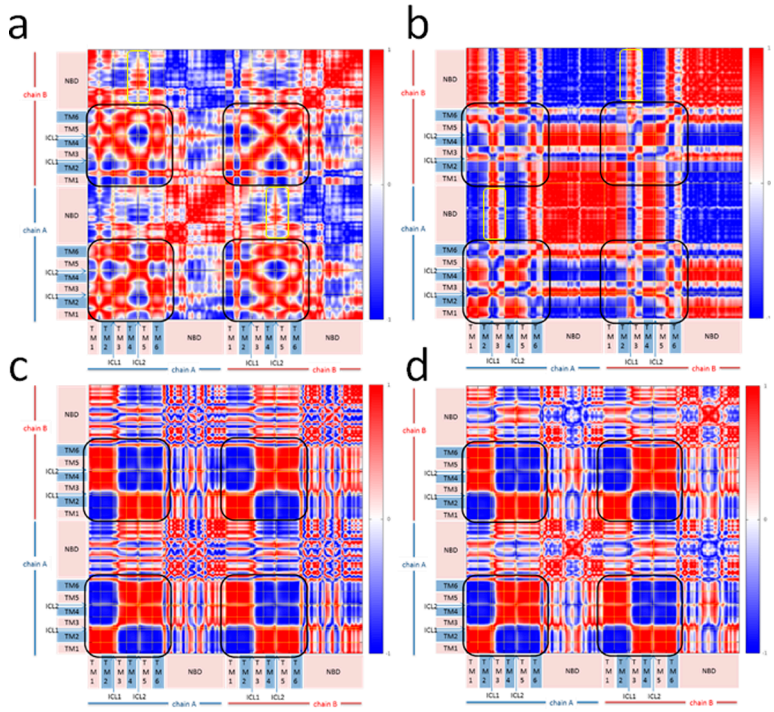

Figure 7 Correlation maps at k=51 (a), 54 (b), 75 (c) and 100 (d).

same wing and negative between different wings. ICL1 and ICL2 also had correlation patterns essentially similar to those at k=3 as mentioned above. A correlation pattern similar to Figure 6b was maintained until the translational forces were put off at step 50×10^5.

Immediately after the ATP node was added (k=51, Fig. 7a), a new feature appeared in the interactions between the ICLs and the NBD regions (yellow square). In the exporters, the ICL2s are domain-swapped, that is, ICL2 from chain A interacts with the NBD of chain B and vice versa (Supplementary Fig. S1) [8]. Due to this fact, there are likely positive correlations between the ICL2 of chain A and the NBD of chain B and between the ICL2 of chain B and the NBD of chain A. This suggests that the NBD and its partner ICL2 were dynamically coupled; thus, this coupling might exert an influence on the motion of the TMDs. However, the inter-TM helix correlation is still positive within each wing in the IF state ($\text{wing}_1^{\text{IF}}$ or $\text{wing}_2^{\text{IF}}$), but it is negative between these wings. These correlation patterns are identical to those found for $k\leq50$, which is consistent with the observation that the TMD structures had not yet changed (Fig. 5a).

At k=54 (Fig. 7b), there appears a strong positive correlation between ICL1 and its partner NBD in both chains A and B (yellow square). This indicates that the contact between ICL1 and its partner NBD becomes stronger, which implies that the protein is ready for the transmission of the NBD's motions to the TM helices. Indeed, the TM helices exhibited characteristic correlation patterns that match neither the pat-

tern expected for the wings in the IF state nor that expected for the OF state. In particular, the behavior of TM3 is unique: a part of TM3 has positive correlations (red) with other TM helices, and its residual part has negative correlations (blue) with them. This indicates that the motion of TM3 is no longer a rigid body-like motion, which may suggest that the flexible motion of this helix is a trigger for the rearrangement of the helix bundle.

At k=75 (Fig. 7c), drastic changes occurred among the TM helices: the inter-TM helix correlation became positive within each wing of the OF state ($wing_1^{OF}$ or $wing_2^{OF}$), but it is negative between these wings. This is quite consistent with the observation that the protein structure was mostly transitioned into the OF structure at this stage (75×10^5th step in Fig. 5). After the complete transition into the OF state (k=100, Fig. 7d), the above correlation patterns were, of course, maintained. Interestingly, at k=75 and 100, the ICLs have positive correlations with their directly linking TM helices: between ICL1 and its two side helices (TM2 and TM3) and between ICL2 and its two side helices (TM4 and TM5). This is in contrast to the cases of k=51 and 54, where the ICLs have positive correlation with their partner NBDs as mentioned above. These observations indicate that the effect of addition of the ATP node is propagated gradually from the NBDs to the TMDs via the ICLs. Another finding is that the intra-NBD correlation pattern is subdivided into three parts at these final stages. In Figure 7c and d (k=75 and 100), the intra- and inter-NBD interactions both are roughly divided into six subdivided regions, except for the mirror image on the upper (or lower) triangle. This is in marked contrast to Figure 7b, where the intra- and inter-NBD interactions are almost entirely positive (red) and negative (blue), respectively. In ABC transporters, each NBD has a consecutive domain arrangement of RecA subdomain–α-helical subdomain–RecA subdomain. In the OF structure (at k=100), the correlation between the α-helical subdomain and each of the RecA subdomains is negative (blue), whereas that between the two RecA subdomains is positive (red). These observations suggest that the intra- and inter-NBD motions become highly organized as a result of the dimerization of the two NBDs.

Energy accumulation in the TM helices

The above results indicate that the IF→OF transition is induced by addition of the ATP nodes; in other words, it is driven by the free energy gain from ATP binding. If so, the ATP energy should be converted into the internal energy of the protein. To examine this, we calculated the distortion energy defined by eq. (9) for each TM helix in the OF state. Then, the structure at k=50 (immediately before addition of the ATP nodes) was chosen as the reference structure. The results for helices TM2~TM6 are shown in Figure 8a, where the calculation for TM1 was not performed because its helix length was too short to contribute to the internal energy. The energy levels of TM2 and TM5 increased in the early time

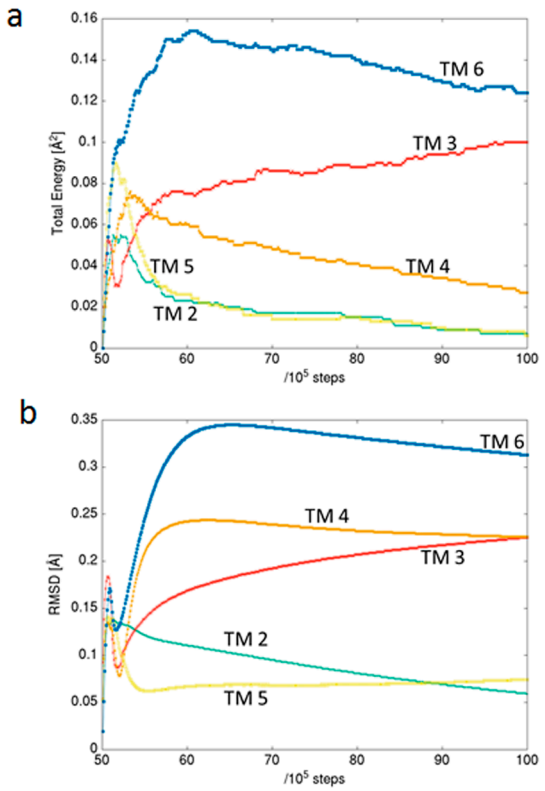

Figure 8 Time evolution of the distortion energy (a) and RMSD (b) of the TM helices.

period (~53×10^5 step) but thereafter, their energy is rapidly released. As a result, the net energy accumulation in these helices is very small. In the case of TM3, a slight energy accumulation and its immediate release occurred within an early short period (51~52×10^5 step), and after that, the energy continuously increased until the protein reached the complete OF state. The rapid energy change in the early period might originate from non-rigid body motion that would induce the rearrangement of the TM helices as described in the analysis of correlated motions (Fig. 7b). In the cases of TM4 and TM6, the energy accumulated in the early period is still substantially stored in the OF state: in particular, TM6 is the maximal contributor to the energy accumulation.

To examine the origin of the energy accumulated by each TM helix, we calculated the RMSD of each helix, where the reference structure was taken to be the same as in the calculation of the distortion energy. As seen from the comparison between Figures 8a and 8b, the behavior of the distortion energy of the TM helices correlates well with that of RMSD, although the amount of energy accumulated in TM4 may be smaller than expected from the change in RMSD. The structural distortions are relatively large in TM3 and TM6. This is consistent with the X-ray structure of MsbA (PDBID: 3B60), where TM3 and TM6 are bent significantly. In contrast, TM2 and TM5 both are not explicitly bent in the experimental structure. Therefore, our coarse-grained model successfully

reproduces the features of the experimental structure of MsbA, and the tendencies of the overall distortion energy changes in the TM helices are thought to be reliable.

Taken together, it can be concluded that the OF state has a higher internal energy than the IF state and that this energy increment comes from the ATP binding energy.

Discussion and Conclusion

Recently, experimental studies based on X-ray diffraction analysis and cryo-electron microscopy have revealed the structures of ABC transporters in various reaction states such as ATP-bound, ADP-bound, and ATP-free [8, 28–31]. However, from these snapshot structures alone, it is difficult to understand the mechanism by which the binding of ATP and its hydrolysis cause the functional motions such as IF→OF and OF→IF transitions, in other words, the chemo-mechanical coupling. To address this issue, we examined how the protein responds to the application of an external perturbation from ATP by solving the nonlinear equation of motion based on ENM. In particular, we focused on the analysis of the IF→OF transition caused by the binding of ATP molecules.

Because of observations that the IF→OF conformational "switch" is dependent on ATP binding at the NBDs, this step is often referred to as the "power stroke" of substrate export [32–36]. Despite the major advances in our understanding of the molecular mechanism of ABC exporters, the process of conformational coupling between the NBDs and TMDs during the power stroke remains unclear. Does the IF→OF transition really occur only by ATP binding at the NBDs without ATP hydrolysis?

Here, we showed that ATP binding alone is sufficient for the occurrence of the IF→OF transition. First, it was found that external force along the x-axis led to their dimerization but never caused motions of the TMDs toward the OF state. Second, the addition of ATP nodes caused opening motions of the TMDs comparable to the experimental structure accompanied by twisting of the NBDs about the x-axis. This result suggests that the interactions of the bound ATP with its surrounding amino acid residues bring about the rotation force about the x-axis. To confirm this, we solved the equation of motion with applying such a force about the x-axis and successfully reproduced the opening of the TMDs. Analysis of the correlated motions suggested that such a rotational motion is transmitted to the ICLs from the NBDs, which in turn causes a rearrangement of the helix bundles and the concomitant opening motion of the TMDs. The first sign of the helix rearrangement was seen in non-rigid body motions of TM3. According to our internal energy evaluation, the OF state is higher than the IF state, which implies that the ATP binding energy is converted into elastic energy of several TM helices, mainly TM3, TM4 and TM6. Net energy accumulation was not observed for TM2 or TM5. These results propose an interesting empirical rule: the elastic energy is accumulated mainly in the helices (TM3, TM4 and TM6) that move from one wing to another wing during the helix bundle rearrangement, while no apparent energy accumulation was observed for TM2 and TM5, which stay in their original wing during the rearrangement. It is likely that the helix rearrangement is driven by the elastic energy accumulated in TM3, TM4 and TM6.

The above results indicate that the conformational changes of NBDs are propagated to the TMDs via the intracellular loops. This is a kind of allosteric communication. Then, the twisting motion of the NBDs plays an important role in the rearrangement of the TM helix bundles and the resultant TMD opening. The importance of twisting motion of the NBDs has already been noted in several previous studies. As described in the introduction, Moradi and Tajkhorshid proposed a 'doorknob' mechanism, which indicates that during the OF→IF transition of MsbA, the opening of the cytoplasmic gate is disfavored when the periplasmic gate is open and facilitated by a twisting motion of the NBDs that involves a dramatic change in their relative orientation [20]. A coarse-grained simulation based on an adaptive anisotropic network model also provided the result that the twisting motion of the NBDs is essential for the occurrence of the IF→OF transition [23]. A new finding from the present study is that rotation of the NBDs around the x-axis is particularly important for the conformational transition. This is consistent with our recent study showing that coupling helix 2 (CH2) of MsbA plays an important role in the occurrence of the "nodding-like" motion, corresponding to the rotation of the NBDs around the x-axis [37]. Another new finding is that the ATP binding energy is converted into distortion energy of several transmembrane helices as described above.

Our present calculations are based on ENM and thus the main results should originate from the inter-residue contact topology. Since most of the ABC exporters have the same structural topology as MsbA, the present results are helpful for understanding the transport mechanism of the other exporters.

Conflict of Interest

The authors declare that they have no conflict of interest.

Acknowledgement

This work was supported by JSPS KAKENHI Grant Numbers JP16H00825 (M. S.) and JP15K00400 (T. F.).

Author Contributions

N. A. performed all the simulations and analyses. T. F. and M. S. directed the entire project and co-wrote the manuscript.

References

[1] Holland, I. B, Cole, S. P. C., Kuchler, K. & Higgins, C. F. *ABC Proteins: From Bacteria to Man* (Academic Press, Amsterdam, 2002).

[2] Linton, K. J. Structure and function of ABC transporters. *Physiology* **22**, 122–130 (2007).

[3] Rees, D. C., Johnson, E. & Lewinson, O. ABC transporters: the power to change. *Nat. Rev. Mol. Cell Biol.* **10**, 218–227 (2009).

[4] Moussatova, A., Kandt, C., O'Mara, M. L.& Tieleman, D. P. ATP-binding cassette transporters in Escherichia coli. *Biochim. Biophys. Acta* **1778**, 1757–1771 (2008).

[5] Gottesman, M. M., Fojo, T. Bates, S. E. Multidrug resistance in cancer: Role of ATP-dependent transporters. *Nat. Rev. Cancer* **2**, 48–58 (2002).

[6] Wong, K., Ma. J., Rothnie, A., Biggin, P. C. & Kerr, I. D. Towards understanding promiscuity in multidrug efflux pumps. *Trend. Biochem. Sci.* **39**, 8–16 (2013).

[7] Hollenstein, K., Dawson, R. J. P. & Locher K. P. Structure and mechanism of ABC transporter proeins. *Curr. Opin. Struct. Biol.* **17**, 412–418 (2007).

[8] Locher, K. P. Mechanistic diversity in ATP-binding cassette (ABC) transporters. *Nat. Struct. Mol. Biol.* **23**, 487–493 (2016).

[9] George, A. M., & Jones, P. M. Perspectives on the structure-function of ABC transporters: The Switch and Constant Contact Models. *Prog. Biophys. Mol. Biol.* **109**, 95–107 (2012).

[10] Wilkens, S. Structure and mechanism of ABC transporters. *F1000Prime Rep.* **7**, 14–22 (2015).

[11] López-Marqués, R. L., Poulsen, L. R., Bailly, A., Geisler, M., Pomorski, T. G. & Palmgren, M. G. Structure and mechanism of ATP-dependent phospholipid transporters. *Biochim. Biophys. Acta* **1850**, 461–475 (2015).

[12] Subramanian, N., Condic-Jurkic, K. & O'Mara, M. L. Structural and dynamic perspectives on the promiscuous transport activity of P-glycoprotein. *Neurochem. Int.* **98**, 146–152 (2016).

[13] Ferreira, R. J., Ferreira, M-J. U. & dos Santos, D. J. V. A. Reversing cancer multidrug resistance: insights into the efflux by ABC transports from in silico studies. *WIREs Comput. Mol. Sci.* **5**, 27–55 (2015).

[14] Liu, H., Li, D., Youyong, L. & Hou, T. Atomistic molecular dynamics simulations of ATP-binding cassette transporters. *WIREs Comput. Mol. Sci.* **6**, 255–265 (2016).

[15] Schlitter, J., Engels, M., Krüger, P., Jacoby, E. & Wollmer, A. Targeted Molecular Dynamics Simulation of Conformational Change-Application to the T↔R Transition in Insulin. *Mol. Simul.* **10**, 291–308 (1993).

[16] Kästner, J. Umbrella sampling. WIREs *Comput. Mol. Sci.* **1**, 932–942 (2011).

[17] Ward, A., Reyes, C. L., Yu, J., Roth, C. B. & Chang, G. Flexibility in the ABC transporter MsbA: Alternating access with a twist. Proc. Natl. Acad. Sci. USA **104**, 19005–19010 (2007).

[18] Weng, J-W., Fan, K-N. & Wang, W-N. The conformational transition pathway of ATP binding cassette transporter MsbA revealed by atomistic simulations. *J. Biol. Chem.* **285**, 3053–3063 (2010).

[19] Moradi, M. & Tajkhorshid, E. Computational recipe for efficient description of large-scale conformational changes in biomolecular systems. *J. Chem. Theory Comput.* **10**, 2866–2880 (2014).

[20] Moradi, M. & Tajkhorshid, E. Mechanistic picture for conformational transition of a membrane transporter at atomic resolution. *Proc. Natl. Acad. Sci. USA* **110**, 18916–18921 (2013).

[21] Tirion, M. M. Large amplitude elastic motions in proteins from a single-parameter, atomic analysis. *Phys. Rev. Lett.* **77**, 1905–1908 (1996).

[22] Atilgan, AR., Durell, S. R., Jernigan, R. L., Demirel, M. C., Keskin, O. & Bahar, I. Anisotropy of fluctuation dynamics of proteins with an elastic network model. *Biophys. J.* **80**, 505–515 (2001).

[23] Xie, X. L., Li, C. H.,Yang, X. Y., Jin. L., Tan, J. J., Zhang, X. Y., *et al*. Allosteric transitions of ATP-binding cassette transporter MsbA studied by the adaptive anisotropic network model. *Proteins* **83**, 1643–1653 (2015).

[24] Togashi, Y. & Mikhailov, A. S. Nonlinear relaxation dynamics in elastic networks and design principles of molecular machines. *Proc. Natl. Acad. Sci. USA* **104**, 8697–8702 (2007).

[25] Cressman, A., Togashi, Y., Mikhailov, A. S. & Kapral, R. Mesoscale modeling of molecular machines: Cyclic dynamics and hydrodynamical fluctuations. *Phys. Rev. E Stat. Nonlin. Soft Matter Phys.* **77**, 050901-1-050901-4 (2008).

[26] Düttmann, M., Togashi, Y., Yanagida, T. & Mikhailov, A. S. Myosin-V as a mechanical sensor: An elastic network study. *Biophys. J.* **102**, 542–551 (2012).

[27] Hsu, W. L., Furuta, T. & Sakurai, M. Analysis of the free energy landscapes for the opening-closing dynamics of the maltose transporter ATPase $MalK_2$ using enhanced sampling molecular dynamics simulation. *J. Phys. Chem. B* **119**, 9717–9725 (2015).

[28] Zhang, Z. & Chen, J. Atomic Structure of the Cystic Fibrosis Transmembrane Conductance Regulator. *Cell* **167**, 1586–1597 (2016).

[29] Liu, F., Zhang, Z., Csanády, L., Gadsby, D. C. & Chen, J. Molecular Structure of the Human CFTR Ion Channel. *Cell* **169**, 85–95 (2017).

[30] Zhang, Z., Liu, F. & Chen, J. Conformational Changes of CFTR upon Phosphorylation and ATP Binding. *Cell* **170**, 483–491 (2017).

[31] Mi, W., Li, Y., Yoon, S. H., Ernst, R. K., Walz, T. & Liao, M. Structural basis of MsbA-mediated lipopolysaccharide transport. *Nature* **549**, 233–237 (2017).

[32] McDevitt, C. A., Crowley, E., Hobbs, G., Starr, K. J., Kerr, I. D. & Callaghan, R. Is ATP binding responsible for initiating drug translocation by the multidrug transporter ABCG2? *FEBS J.* **275**, 4354–4362 (2008).

[33] Dawson, R. J., & Locher, K. P. Structure of the multidrug ABC transporter Sav1866 from Staphylococcus aureus in complex with AMP-PNP. *FEBS Lett.* **581**, 935–938 (2007).

[34] Higgins, C. F. & Linton, K. J. The ATP switch model for ABC transporters. *Nat. Struct. Mol. Biol.* **11**, 918–926 (2004).

[35] Smith, P. C., Karpowich, N., Millen, L., Moody, J. E., Rosen, J., Thomas, P. J., *et al.* ATP binding to the motor domain from an ABC transporter drives formation of a nucleotide sandwich dimer. *Mol. Cell*. **10**, 139–149 (2002).

[36] Moody, J. E., Millen, L., Binns, D., Hunt, J. F. & Thomas, P. J. Cooperative, ATP-dependent association of the nucleotide binding cassettes during the catalytic cycle of ATP-binding cassette transporters. *J. Biol. Chem.* **277**, 21111–21114 (2002).

[37] Furuta, T., Yamaguchi, T., Kato, H. & Sakurai, M. Analysis of the structural and functional roles of coupling helices in the ATP-binding cassette transporter MsbA through enzyme assays and molecular dynamics simulations. *Biochemistry* 53, 4261–4272 (2014).